Suppression of the Berezinskii-Kosterlitz-Thouless and quantum phase transitions in two-dimensional superconductors by finite-size effects

T. Schneider* and S. Weyeneth

Physik-Institut der Universität Zürich, Winterthurerstrasse 190, CH-8057 Zürich, Switzerland

(Received 8 July 2014; revised manuscript received 22 July 2014; published 1 August 2014)

We perform a detailed finite-size scaling analysis of the sheet resistance in Bi films and the $LaAlO_3/SrTiO_3$ interface in the presence and absence of a magnetic field applied perpendicular to the system. Our main aim is to explore the occurrence of Berezinskii-Kosterlitz-Thouless (BKT) and quantum phase transition behavior in the presence of limited size, stemming from the finite extent of the homogeneous domains or the magnetic field. Moreover we explore the implications thereof. Above an extrapolated BKT transition temperature, modulated by the thickness d, gate voltage V_g, or magnetic field H, we identify a temperature range where BKT behavior occurs. Its range is controlled by the relevant limiting lengths, which are set by the extent of the homogeneous domains or the magnetic field. The extrapolated BKT transition lines $T_c(d,V_g,H)$ uncover compatibility with the occurrence of a quantum phase transition where $T_c(d_c,V_{gc},H_c)=0$. However, an essential implication of the respective limiting length is that the extrapolated phase transition lines $T_c(d,V_g,H)$ are unattainable. Consequently, given a finite limiting length, BKT and quantum phase transitions do not occur. Nevertheless, BKT and quantum critical behavior is observable, controlled by the extent of the relevant limiting length. Additional results and implications include: the magnetic-field-induced finite-size effect generates a flattening out of the sheet resistance in the $T\to 0$ limit, while in zero field it exhibits a characteristic temperature dependence and vanishes at $T=0$ only. The former prediction is confirmed in both the Bi films and the $LaAlO_3/SrTiO_3$ interface as well as in previous studies. The latter is consistent with the $LaAlO_3/SrTiO_3$ interface data, while the Bi films exhibit a flattening out.

DOI: 10.1103/PhysRevB.90.064501 PACS number(s): 74.40.−n, 74.78.−w, 64.60.Ht

I. INTRODUCTION

Over the last two decades, electrical transport measurements of thin films near the onset of superconductivity have been studied extensively [1–4]. Crucial observations include: the sheet resistance in zero magnetic field remains nearly temperature independent at the lowest attained temperature [5,6] and remains ohmic below the expected normal state to superconductor transition temperature T_c [7–9]; a magnetic field applied perpendicular to the film generates a flattening out of the sheet resistance in the $T\to 0$ limit [10–13]; the occurrence of a smeared Nelson-Kosterlitz jump [14] in the superfluid density in the absence [15,16] and presence of a magnetic field [17]. Interpretations of the saturation of the sheet resistance in the $T\to 0$ limit include the formation of a metallic phase [10–12,18], the occurrence of quantum tunneling of vortices [6,11], and the failure to cool the electrons [19].

On the other hand, more than three decades ago, Beasley, Mooij, and Orlando [20] suggested that the Berezinskii-Kosterlitz-Thouless [21,22] (BKT) transition may be observable in sufficiently large and thin superconducting systems. They showed whenever the effective magnetic penetration depth $\lambda_{2D}=\lambda^2/d$ exceeds the sample size $[W_s,L_s]$, where λ is the magnetic penetration depth, d the thickness, W_s the width, and L_s the length of the system, the vortices interact logarithmically over the entire sample, a necessary condition for a BKT transition to occur. Indeed, as shown by Pearl [23], vortex pairs in thin superconducting systems (charged superfluid) have a logarithmic interaction energy out to the characteristic length $\lambda_{2D}=\lambda^2/d$, beyond which the interaction energy falls off as $1/r$. Accordingly, as λ_{2D} increases the diamagnetism of the superconductor becomes less important and the vortices in a thin superconducting film become progressively like those in ^{4}He films. Invoking the Nelson-Kosterlitz relation [14] in the form $\lambda_{2D}=\lambda^2(T_c)/d=\Phi_0^2/(32\pi^2 k_B T_c)$, it is readily seen that for sufficiently low T_c's, the condition $\lambda_{2D}>[W_s,L_s]$ is in practice accomplishable. Indeed, $T_c=1$ K yields $\lambda_{2D}\simeq 0.98$cm. Additional limiting lengths include the magnetic length $L_H\propto(\Phi_0/H)^{1/2}$ associated with fields applied perpendicular to the film and in the case of ac measurements $L_f\propto f^{-1/2}$ where f denotes the frequency. Concentrating on dc measurements of the sheet resistance one expects that the dimension of the homogeneous domains L_h sets in zero magnetic field the smallest size so that $L=L_h=\min[W_s,L_s,\lambda_{2D},L_h]$. As the magnetic field increases this applies as long as $L<L_H$, while for $L>L_H$ the magnetic field sets the limiting length. It controls the density of free vortices n_F, which determines the sheet resistance ($R\propto n_F$) as well as the correlation length ($\xi\propto n_F^{-1/2}$) at and above T_c [24,25]. Accordingly, the correlation length cannot grow beyond L. In this context it is important to recognize that the finite-size scaling approach adopted here is compatible with the Harris criterion [26,27], stating that short-range correlated and uncorrelated disorder is irrelevant at the BKT critical point, contrary to approaches where the smearing of BKT criticality is attributed to a Gaussian-like distribution of the bare superfluid stiffness around a given mean value [28]. In this context it should be recognized that irrelevance of this disorder applies to the universal properties, while the nonuniversal parameters, including T_c and the vortex core radius, may change. The finite-size effects stemming from the limited extent of the homogeneous domains or the applied

*toni.schneider@swissonline.ch

magnetic field have a profound influence on the observation of the BKT behavior and have been studied intensely in recent years [9,24,25,29,30]. On the other hand, over the years, consistency with BKT behavior has been reported in thin films [17,29–35], and in systems exhibiting interfacial superconductivity [7–9,24].

Here we extend previous work [9,24,29,30] and analyze the sheet resistance data of Bi films [6] and the $LaAlO_3/SrTiO_3$ interface [8,9] using the finite-size scaling formulas appropriate for the BKT transition, which include multiplicative corrections when present [24,25]. These systems have been chosen because the data comprise the low-temperature limit, namely $T \ll T_c$ where T_c is the extrapolated BKT transition temperature attained in the limit of an infinite limiting length L.

The paper is organized as follows. In Sec. II we sketch the finite-size scaling behavior of the sheet resistance adapted to the BKT critical point and present the correspondent analysis of the thickness tuned Bi films and the gate voltage tuned $LaAlO_3/SrTiO_3$ interface, in the presence and absence of a magnetic field, applied perpendicular to the film or interface. We observe remarkable consistency with the finite-size scaling predictions. In the presence and absence of a magnetic field we identify a temperature range above the extrapolated T_c where BKT behavior occurs. This temperature range is controlled by the relevant limiting length. In zero magnetic field it is the extent of the homogeneous domains. It turns out to decrease with the thickness d or gate voltage V_g tuned reduction of $T_c(d,V_g)$. The survival of BKT behavior in applied magnetic fields implies a smeared sudden drop in the superfluid stiffness at $T_c(H)$, where it adopts the universal value given by the Nelson-Kosterlitz relation [14]. Recently, this behavior has been observed in MoGe and InO_x thin films by means of low-frequency measurements of the ac conductivity [17]. Analogously, provided there is a temperature range above $T_c(d,V_g)$ where BKT behavior is present, the smeared jump should also occur in zero field, as observed in various films [15,16]. An essential implication of the respective limiting length is that the extrapolated phase transition lines $T_c(d,V_g,H)$ are unattainable. As a consequence the occurrence of BKT transitions is suppressed and with that the occurrence of quantum phase transitions in the limit $T_c(d,V_g,H) \to 0$ as well. Nevertheless, in agreement with previous studies [9,29,30,35], the lines $T_c(d,V_g,H)$ exhibit the characteristic quantum critical properties. Additional implications of finite-size scaling adapted to the BKT transition include: the magnetic-field-induced finite-size effect generates a flattening out of the sheet resistance in the $T \to 0$ limit, while in zero field it exhibits a characteristic temperature dependence and vanishes at $T = 0$ only. The former prediction is confirmed in both the Bi films and the $LaAlO_3/SrTiO_3$ interface, as well as in previous studies [10–12]. The latter is consistent with the $LaAlO_3/SrTiO_3$ interface data, while the Bi films exhibit a flattening out. Finally we explore the limitations of the quantum scaling approach [36].

II. THEORETICAL BACKGROUND AND DATA ANALYSIS

Since only the motion of free vortices dissipate energy, the sheet resistance should be proportional to the free vortex density [37]

$$R(T) \propto n_F(T). \tag{1}$$

On the other hand, dynamic scaling predicts the relationship [38]

$$R(T) \propto \xi_+^{-z}(T), \tag{2}$$

between the sheet resistance above T_c and the corresponding correlation length [39]

$$\xi_+(T) = \xi_0 \exp\left(\frac{2\pi}{bt^{1/2}}\right), t = T/T_c - 1. \tag{3}$$

z is the dynamic critical exponent, the amplitude ξ_0 is related to the vortex core radius and b is a nonuniversal parameter related to the vortex core energy [9,40]. However, approaching T_c from above, the aforementioned limiting lengths imply that the correlation length $\xi_+(T)$ cannot grow beyond $L = L_h = \min[W_s, L_s, \lambda_{2D}, L_h]$. According to this a finite-size effect becomes visible around $T^* > T_c$ where

$$\xi_+(T^*) \simeq L. \tag{4}$$

This leads to a characteristic size dependence of the sheet resistance [9,24,25,29,30]. Indeed, Eqs. (2) and (4) imply that for $z = 2$ at $T^* > T_c$ the sheet resistance adopts the size dependence

$$\frac{\sigma(T^*)}{\sigma_0} = \frac{R_0}{R(T^*)} = \left(\frac{L}{\xi_{0+}}\right)^2. \tag{5}$$

To illustrate the experimental situation we consider next the sheet resistance data of Lin *et al.* [6] for Bi films of various thickness and the heat conductance data of Agnolet *et al.* [41] for a 23.42 Å thick ^{4}He film. Both, the sheet resistance in thin superconducting films and the heat resistance in ^{4}He film are supposed to be proportional to the to the free vortex density n_F so that according to Eq. (2) the respective conductance scales of a homogeneous film with infinite extent scales for $z = 2$ as

$$\frac{\sigma(T)}{\sigma_0} = \frac{R_0}{R(T)} = \exp(b_R t^{-1/2}), \tag{6}$$

where

$$b_R = 4\pi/b. \tag{7}$$

Supposing that the BKT regime is attainable, b_R is nearly independent of film thickness, R_0 and T_c adopt the appropriate values, the data plotted as $\sigma(T)/\sigma_0$ vs $t^{-1/2}$ should then fall on the single curve $\exp(b_R t^{-1/2})$. In Fig. 1(a) we depicted this plot for the Bi films. As $t^{-1/2}$ increases and with that T_c is approached the data no longer collapse, but run away and flatten out at $\sigma(T)/\sigma_0$ values, which increase with film thickness d. This behavior points to a finite-size effect where the correlation length $\xi_+(T)$ cannot grow beyond the limiting length L so that Eq. (5) applies. As a result the flattening out is controlled by the ratio L/ξ_{0+} which increases with film thickness and T_c. In Fig. 1(b) we plotted the thickness dependence of R_0 and of the extrapolated BKT transition line $T_c(d)$. Apparently the decrease of T_c with reduced film thickness points to a quantum phase transition at a critical thickness dc where $T_c(d_c) = 0$.. Because the extrapolated BKT transition temperatures are not attainable due to the

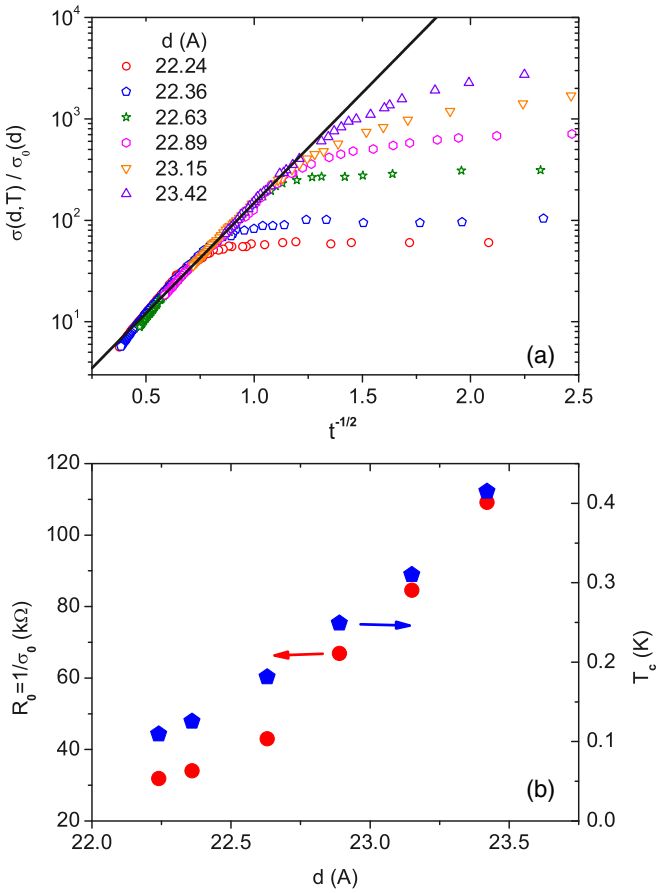

FIG. 1. (Color online) (a) Normalized sheet conductance $\sigma(d,T)/\sigma(d)$ of Bi films of thickness d vs $t^{-1/2} = (T/T_c - 1)^{-1/2}$ derived from Lin *et al.* [6]. The solid line is the BKT behavior $\sigma(d,T)/\sigma_0(d) = \exp(b_R t^{-1/2})$ for a homogenous and infinite system with $b_R = 5$. (b) Thickness dependence of the extrapolated T_c and R_0.

limiting length L, it follows that these transitions, as well as the possible quantum phase transition at $T_c(d_c) = 0$ are suppressed. Nevertheless, slightly above T_c, where the data tend to collapse on the BKT line, BKT fluctuations are present. This collapse attests to the consistency with the universal and characteristic form of the BKT correlation length [Eq. (6)], while the nonuniversal parameters T_c and R_0 depend on the film thickness d [see Fig. 1(b)]. The reduction of T_c and R_0 is attributable to disorder and quantum fluctuations. In particular, the strength of disorder is expected to increase with reduced film thickness d. To quantify this expectation we consider

$$k_F l = (h/e^2)/R_n, \tag{8}$$

where k_F denotes the Fermi wave number, l the electron mean free path, and R_n the normal state sheet resistance. As disorder increases the mean free path l diminishes, $k_F l$ decreases, and the strength of disorder increases. In the Bi films considered here $k_F l$ varies from 3.8 for $d = 22.2$ Å to 17.4 for $d = 23.42$ Å. Accordingly, the strength of the disorder increases substantially with reduced film thickness or T_c. Nevertheless, it does not affect the universal BKT properties but renormalizes the nonuniversal parameters.

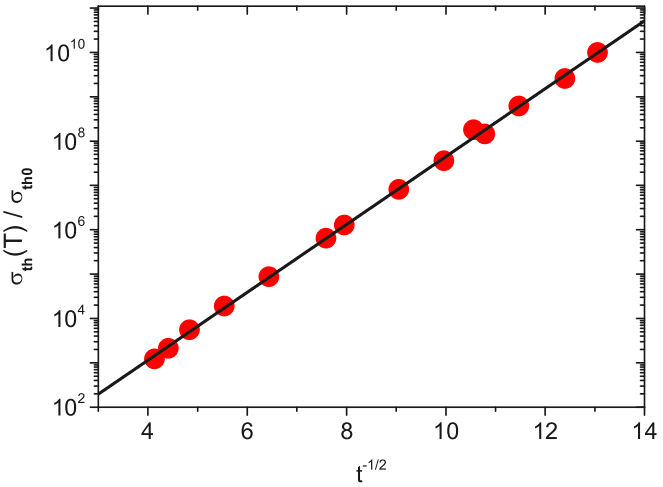

FIG. 2. (Color online) Thermal conduction $\sigma_{th}(T)/\sigma_{th0}$ of a 23.42 Å thick ^{4}He film vs $t^{-1/2}$ with $T_c = 1.2794$ K taken from Agnolet *et al.* [41]. The solid line is the BKT behavior $\sigma_{th}/\sigma_{th0} = \exp(b_R t^{-1/2})$ with $b_R = 1.762$ and $\sigma_{th0} = \exp(-24.13954) = 3.283 \times 10^{-11}$ W/K.

To classify the relevance of the finite-size effect in the Bi films we show in Fig. 2 the corresponding scaling plot of the thermal conductance of a ^{4}He film. Although the data attain the transition temperature rather closely there is now sign of a flattening out up to $t^{-1/2} \simeq 13$, while in the Bi films it sets in around $0.4 \lesssim t^{-1/2} \lesssim 0.75$ [Fig. 1(a)], depending on the film thickness. Taking this dramatic difference as a generic fact, a finite scaling analysis of the sheet resistance data appears to be inevitable to uncover BKT behavior.

So far we considered finite-size effects occurring at and above the transition temperature T_c. In Fig. 3 we depicted $R(d,T)/R_0$ vs $T_c(d)/T$ for the Bi films derived from Lin *et al.* [6]. As T approaches $T_c(d)$ the data no longer collapse, but run away from the BKT behavior and flatten out at $R(d,T)/R_0(d)$ values, which decrease with film thickness d.

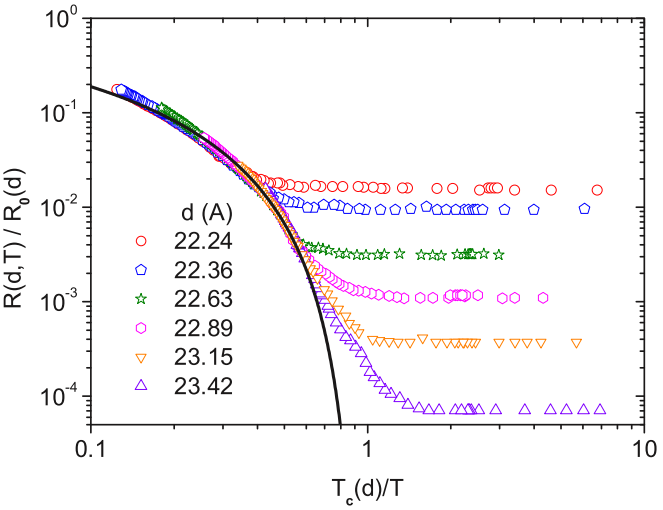

FIG. 3. (Color online) $R(d,T)/R_0$ vs $T_c(d)/T$ for the Bi films derived from Lin *et al.* [6] The solid line is the BKT behavior $R(T)/R_0 = \exp(-b_R(T/T_c - 1)^{-1/2})$ with $b_R = 5$.

The flattening out extending above $T_c(d)/T > 1$ points then to a finite-size effect below $T_c(d)$ as well. However, below T_c the dynamic scaling relation (2) is no longer applicable because the correlation length is infinite there owing to the divergence of the susceptibility [22].

The BKT theory predicts that below T_c all vortices are bound in pairs by the logarithmic vortex interaction, whereupon the linear sheet resistance is zero. Instead there is a nonlinear dependence of the voltage on current since the current can unbind weakly bound pairs [37]. Contrariwise, in a finite sample there will be a population of free vortices at and below the vortex unbinding transition temperature T_c [25,32,33]. In this temperature regime the linear relationship (1) between sheet resistance and free vortex density still applies, while Eq. (2), relating the sheet resistance to the correlation length [Eq. (3)], applies at and above T_c only. To provide a rough estimate of the free vortex density we note that at low temperatures the energy change resulting from adding a single vortex in a system of size L is given by $\Delta E = (J(T)/2)\int_0^{2\pi} d\Theta \int_{\xi_0}^{L} RdR/R^2 = \pi J(T)\ln(L/\xi_{0-})$ [42], where ξ_0 is the vortex core radius and

$$J(T) = \hbar^2\rho_s(T)/2m = d\Phi_0^2/(16\pi^3\lambda^2(T)), \tag{9}$$

denotes the superfluid stiffness at low temperatures ($T \ll T_c$). An estimate for the free vortex density follows then from the probability of finding a free vortex from the Boltzmann factor

$$P(T) \propto n_F(T) \propto \exp(-\Delta E/k_BT) = (\xi_0/L)^{\pi J(T)/k_BT}. \tag{10}$$

Using Eq. (1) we obtain,

$$R(T) \propto n_F(T) \propto (\xi_0/L)^{\pi J(T)/k_BT} \quad : T \ll T_c. \tag{11}$$

Invoking the universal Nelson-Kosterlitz relation [14]

$$k_BT_c = \frac{\pi}{2}J(T_c^-), \tag{12}$$

the temperature range of validity is then restricted to $T \ll T_c = \pi J(T_c^-)/2k_B$. As it should be, for an infinite system, n_F is zero for $T \leqslant T_c$. But if the limiting length L is finite, the free vortex density vanishes at zero temperature only. This implies an ohmic tail in the IV characteristic below the extrapolated T_c [7,32,33] and impedes a normal state to superconductor transition at finite temperature in a strict sense. In this context it is important to recognize that the standard finite-size scaling outlined above neglects the multiplicative logarithmic corrections associated with BKT critical behavior [25,43]. A recent renormalization group treatment yields for $z = 2$ and free boundary conditions [25]

$$R(T) \propto \begin{cases} (\xi_0/L)^{\pi J(T)/k_BT} & : L \gtrsim \xi_-(T) \\ (\xi_0/L)^2/\ln((L_{\rm lim}/\xi_0)/b_0) & : L \lesssim \xi_+(T) \end{cases}, \tag{13}$$

where

$$\xi_-(T) = \xi_0 \exp\left(\frac{1}{b|t|^{1/2}}\right), \tag{14}$$

is a diverging length below T_c [39]. With Eq. (3) it follows that this thermal length is much smaller than the correlation length $\xi_+(T)$ for the same $|t|$, because

$$\xi_+(t)/\xi_0 = [\xi_-(|t|)/\xi_0]^{2\pi}. \tag{15}$$

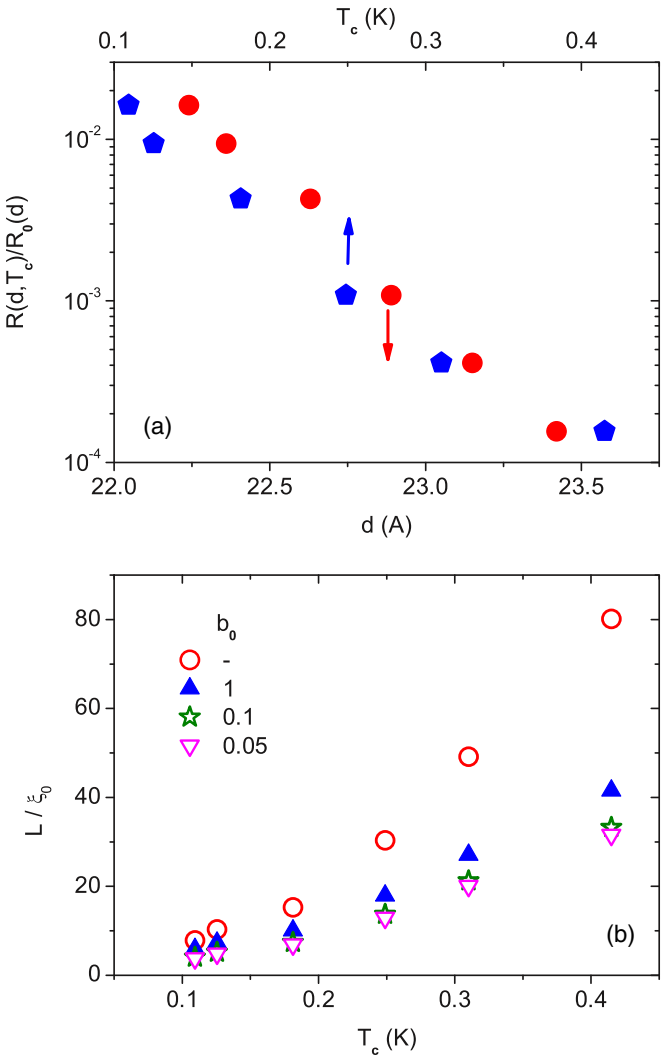

FIG. 4. (Color online) (a) $R(d,T)/R_0(d)$ vs T_c and d derived from the data shown in Fig. 3; (b) Estimates for the ratio L/ξ_0 between correlation length and vortex core radius without the multiplicative logarithmic correction term (◯) and with this correction for different b_0 values entering Eq. (16).

The parameter b_0 is fixed by the initial conditions of the renormalization group equations, [25] while the derivation of Eq. (11) identifies ξ_0 as vortex core radius. Furthermore, there is the upper bound $b_0 < L/\xi_{0-}$ because $R(T) > 0$. Taking the multiplicative logarithmic correction into account Eq. (5) transforms with Eq. (13) to

$$\frac{R(T_c)}{R_0} = \frac{\sigma_0}{\sigma(T_c)} = \left(\frac{\xi_0}{L}\right)^2 \frac{1}{\ln[(L/\xi_0)/b_0]}, \tag{16}$$

valid at $T \simeq T_c$.

Given $R(T_c)/R_0$ and b_0, estimates for $L_{\rm lim}/\xi_{0-}$ are then readily obtained. Figure 4(a) depicts the T_c and d dependence of $R(T_c)/R_0$ derived from Fig. 3, and the resulting T_c dependence of $L_{\rm lim}/\xi_{0-}$ is shown in Fig. 4(b) for $b_0 = 0.05, 0.1$ and 1 in comparison with the neglect of the multiplicative logarithmic correction. These b_0 values satisfy the lower bound $b_0 < L/\xi_0$ resulting from the requirement, $R(d,T_c)/R_0(d) > 0$. Furthermore, $b_0 = 0.05$ is comparable to $b_0 \approx 0.07$, derived

from large-scale numerical simulations [25]. Striking features include the substantial decline of the ratio between limiting length and vortex core radius, L/ξ_0, with decreasing T_c, and the comparably low $L/\xi_0 < 80$ values. Indeed, the runaway is controlled by the magnitude of L/ξ_0. The ^{4}He data shown in Fig. 2 do not exhibit a sign of flattening out up to $\sigma_{th}(T)/\sigma_{th0} = 10^{10}$, yielding with Eq. (5) the lower bound $L/\xi_0 \gtrsim 10^5$. According to this, the runaway observed in Fig. 1(a) and Fig. 3 stems from a limiting length L where the ratio L/ξ_0 decreases with film thickness. Nevertheless, there is a temperature range where consistency with BKT behavior is observed, but in a strict sense a normal state to superconductor BKT transition is suppressed. As a consequence, there is also no film thickness driven quantum phase transition where the phase transition line $T_c(d)$ ends at $T_c(d_c) = 0$ vanishes at a critical film thickness d_c, as could be anticipated from the thickness dependence of the extrapolated T_c shown in Fig. 1(b).

An essential issue left is the elucidation of the limiting length $L_{\min}$. In principle the magnetic-field-induced finite-size effect offers a direct estimate. A magnetic field applied perpendicular to the film leads to the limiting length [24]

$$L_H = \left(\frac{\Phi_0}{aH}\right)^{1/2}, \tag{17}$$

where $a \approx 4.8$ fixes the mean distance between vortices. It prevents the divergence of the correlation length at the extrapolated T_c. In analogy to Eq. (5) the sheet resistance is then expected to scale as

$$R(H,T_c) = \frac{1}{\sigma(H,T_c)} = \frac{f}{L_H^2} = \frac{afH}{\Phi_0}, \tag{18}$$

for $z = 2$ and low fields applied perpendicular to the film [24,25]. In contrast to the zero-field scaling form (13), this law holds below T_c as well and the additive correction to the leading power law dependence is weak [25]. The magnetic field induced finite sets then the limiting length as long as $L_H \propto H^{-1/2} < L$ whereby L_H increases with decreasing field and approaches L. Here a runaway from the scaling behavior (18) sets in at H^* providing for L the estimate

$$L = \left(\frac{\Phi_0}{aH^*}\right)^{1/2}. \tag{19}$$

In Fig. 5 we depicted the magnetic field dependence of the sheet conductivity of the 23.42 Å thick Bi film at $T = 0.1$ K and 0.2 K where the latter is close to the extrapolated T_c. Even though the data are rather sparse we observe in a intermediate magnetic field range consistency with the predicted linear and nearly temperature-independent field dependence of the sheet resistance. Now, we focus on the low field behavior of the conductivity shown in Fig. 5. The run away from the $1/H$ dependence of the sheet conductivity occurs around $H = 0.01$ $T \simeq H^*$, yielding with Eq. (19) for the limiting length the estimate

$$L \simeq 208 \text{ Å}. \tag{20}$$

With $L_{\min}/\xi_0 \simeq 32$, taken from Fig. 4(b), we obtain for the magnitude of the radius of the vortex core radius

$$\xi_0 \simeq 6.5 \text{ Å}. \tag{21}$$

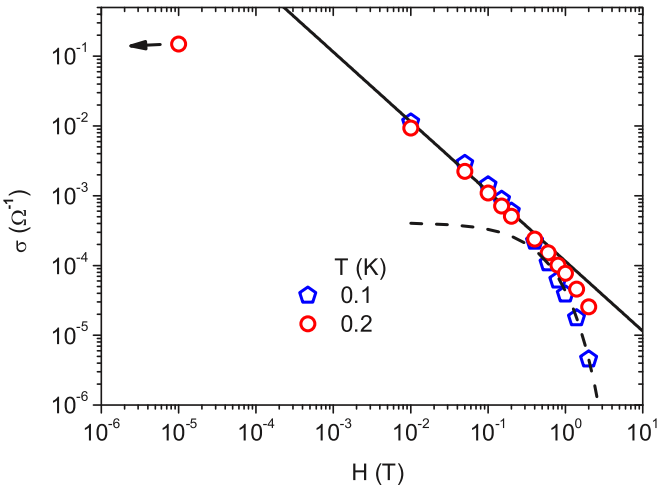

FIG. 5. (Color online) Sheet conductivity σ of the 23.42 Å thick Bi film vs magnetic field H at $T = 0.1$ K and 0.2 K derived from Lin *et al.* [6]. The solid line is Eq. (18) in the from $\sigma = \widetilde{\sigma}/H$ where $\widetilde{\sigma} = 1.15 \times 10^{-4}$ (Ω^{-1}T). The dashed line is Eq. (21) with $\overline{\sigma}_0 = 4.12 \times 10^{-4}$ Ω^{-1} and $\overline{a} = 2.25$ T^{-1}. The arrow indicates that this data point marks the zero-field value of the sheet conductivity.

The deviations from the finite-size scaling behavior at higher fields are not unexpected because with increasing magnetic field the BKT regime is gradually left and he isotherms cross around $H = H_c \simeq 0.4$ T, signaling the occurrence of a magnetic field driven quantum phase transition. In addition Eq. (18) captures the leading field dependence only. In the field range where it applies the plot σ vs $1/H$ shown in Fig. 5 also reveals a nearly temperature-independent coefficient of proportionality $\widetilde{\sigma}$. It implies that the temperature dependence of the sheet resistance at fixed field flattens out, as observed in the 23.42 Å thick Bi film, [6]. Analogous behavior was also observed in MoGe films [11] and Ta films [12] in a field range where the magnetic-field-induced finite-size scaling approach is no longer applicable. Indeed, in the MoGe films the temperature-independent sheet resistance obeys the empirical form [11]

$$\sigma(H) = \overline{\sigma}_0 \exp(-\overline{a}H). \tag{22}$$

In the present case it applies according to Fig. 5 at best above the critical field only. The unusual empirical form was attributed to dissipative quantum tunneling of vortices from one insulating patch to another.

As the estimates for $L_{\min}$ and ξ_0 stem from rather sparse data a reliability check is inevitable. For this purpose we consider the temperature dependence of the correlation length ξ_+ [Eq. (3)] of the 23.42 Å thick Bi film in terms of $\xi_+(T)$ vs $t^{-1/2}$ with $\xi_0 = 6.5$ Å shown in Fig. 6. As ξ_+ growth with increasing $t^{-1/2}$ it approaches the limiting length $L = 208$ Å at $t^{-1/2} \simeq 1.38$, the range where in this film the run away from BKT behavior occurs [see Fig. 1(a)]. Accordingly, we established for the 23.42 Å thick Bi-film reasonable consistency between the estimates for the vortex core radius ξ_0 and the limiting length L, derived from the magnetic-field-induced finite-size effect, and the observed zero-field behavior of the sheet resistance. Unfortunately, this estimation of ξ_0 and L is restricted to this film because the magnetic field dependence

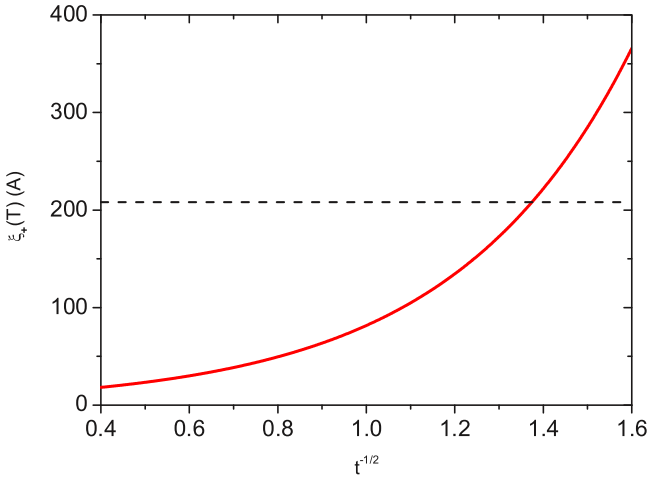

FIG. 6. (Color online) Correlation length $\xi_+ = \xi_0 \exp(2\pi(bt)^{-1/2})$ vs $t^{-1/2}$ of the 23.42 Å thick Bi film with $\xi_0 = 6.5$ Å and $2\pi/b = b_R/2 = 2.5$. The dashed line marks $L = 208$ Å. The crossing point at $t^{-1/2} \simeq 1.38$ corresponds to $T_c/T \simeq 0.66$.

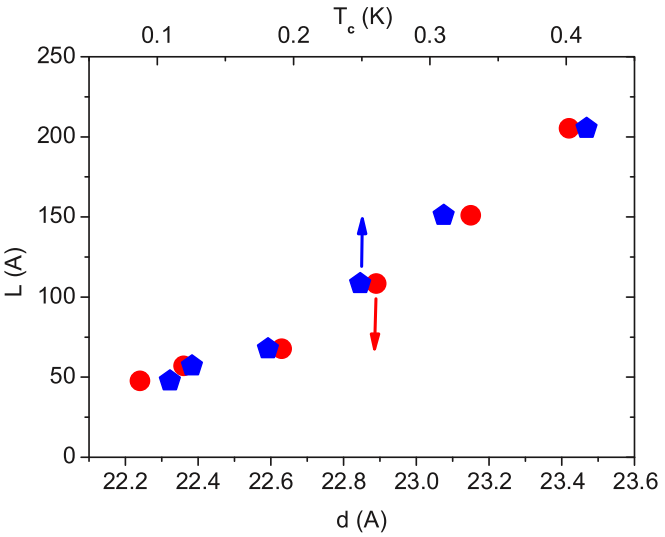

FIG. 7. (Color online) T_c and film thickness dependence of the limiting length L of the Bi films derived from the L/ξ_0 estimates shown in Fig. 4(b) for $b_0 = 0.05$ and $\xi_0 = gT_c^{-1/2}$ with $g = 4.19$ ÅK$^{1/2}$.

of the sheet resistance appears to be missing for the other films. In any case, the rather small limiting length $L = 208$ Å points to an inhomogeneous film, with homogeneous patches of dimension $L = L_h$.

In this context it should be kept in mind that there is the Harris criterion [26,27], stating that short-range correlated and uncorrelated disorder is irrelevant at the unperturbed critical point, provided that $\nu > 2/D$, where D is the dimensionality of the system and ν the critical exponent of the finite-temperature correlation length. With $D = 2$ and $\nu = \infty$, appropriate for the BKT transition [22], this disorder should be irrelevant. Given the irrelevance of disorder, the reduction of the ratio L/ξ_0 with reduced film thickness or transition temperature [see Fig. 4(b)] is then attributable to: (i) increasing vortex core radius ξ_0 with reduced T_c combined with a thickness-independent L; (ii) a limiting length L, which decreases with film thickness combined with a T_c-independent ξ_0; (iii) a thickness dependence of both, L and ξ_0, such that the ratio L/ξ_0 decreases with reduced transition temperature. Because the vortex core radius is known to increase with reduced T_c as $\xi_0 \propto T_c^{-1/z}$ with $z = 2$ [44,45], we are left with options (i) and (iii). In order to discriminate between these options we estimate $\xi_0(T_c)$ from the respective data for the 23.42 Å thick Bi film, namely $\xi_0 = 6.5$ Å and $T_c = 0.41$ K, yielding $\xi_0 = gT_c^{-1/2}$ with $g = 4.19$ ÅK$^{1/2}$. The rough estimates for the thickness and T_c dependence of L shown in Fig. 7 are then readily obtained from the L/ξ_0 values depicted in Fig. 4(b). In spite of the small total thickness increment of 1.18 Å there is a strong thickness dependence of L, ranging from 50–200 Å. Direct experimental evidence for superconducting patches with an extent of 100 Å embedded in an insulating background stems from scanning tunneling spectroscopy investigations on TiNi [46] and InO_x [47] films. However, it should be kept in mind that transport measurements are sensitive to the phase and tunneling experiments to the magnitude of the order parameter. Furthermore, scanning SQUID measurements at the interface $LaAlO_3/SrTiO_3$ uncovered superconducting regions occupying only a small fraction of the areas measured. In addition there are magnetic regions with patches of ferromagnetic regions coexisting with a higher density of much smaller scale domains of fluctuating local magnetic moments [48].

To explore the finite-size scenario further we turn to the interface between $LaAlO_3$ and $SrTiO_3$, two excellent band insulators. It was shown that the electric-field effect can be used to map the phase diagram of this interface system revealing, depending on the gate voltage, a smeared BKT transition, and evidence for quantum critical behavior [8,9]. Here we revisit the analysis of the temperature and gate voltage dependence of the sheet resistance data by invoking the approach outlined above. In Fig. 8(a) we depicted $R(V_g,T)/R_0$ vs $T_c(V_g)/T$ and in Fig. 8(b) the gate voltage dependence of the extrapolated transition temperature T_c and amplitude R_0. As $T_c(V_g)/T$ increases Fig. 8(a) uncovers a flow to and away from the BKT behavior. As $T_c(V_g)/T$ decreases for fixed T_c the BKT regime is left, while the rounding of the transition leads with increasing $T_c(V_g)/T$ to a flow away from criticality. Nevertheless, in an intermediate $T_c(V_g)/T$ regime the data tend to collapse on the characteristic BKT line. Thus, in analogy to the Bi films, the collapse attests again to consistency with the universal and characteristic form of the BKT correlation length [Eq. (6)], while the nonuniversal parameters T_c and R_0 depend in the present case on the gate voltage [see Fig. 8(b)]. Their reduction points to the occurrence of a gate voltage tuned quantum phase transition around $Vg \simeq -100$ V where the extrapolated transition temperature vanishes. Using Eq. (8) we find that $k_F l$ varies from 8.5 at $V_g = 80$ V to 13.7 for $V_g = +80$ V. Accordingly, disorder is present; its strength is comparable to that in the Bi films but increases only slightly by approaching the extrapolated quantum phase transition. In any case, it does not affect the universal BKT properties but renormalizes the nonuniversal parameters.

To unravel the consistency of the rounded transitions with a finite-size effect, we invoke Eq. (16) to estimate the ratio

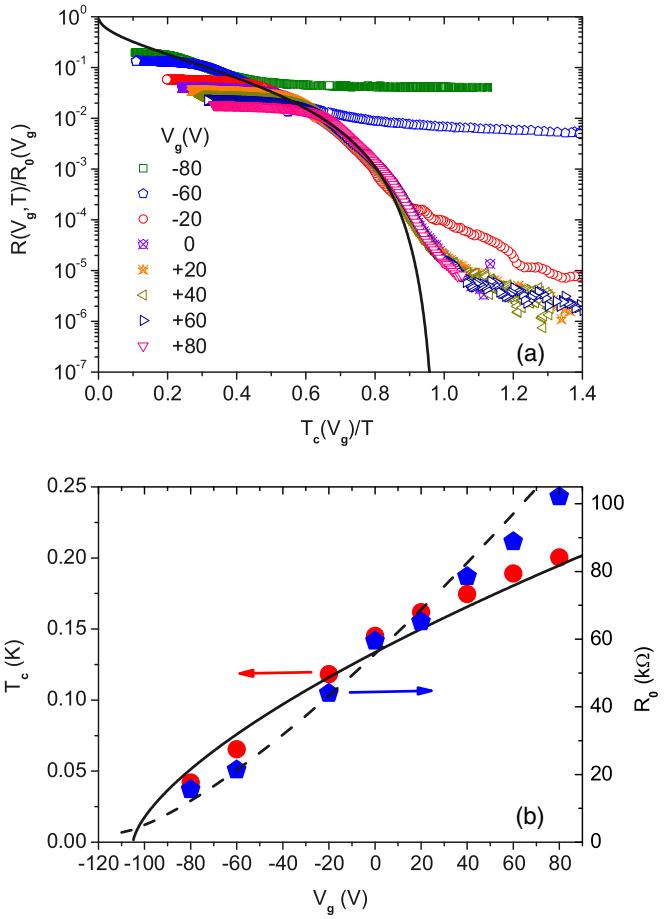

FIG. 8. (Color online) (a) Normalized sheet resistance $R(V_g,T)/R_0(V_g)$ vs $T_c(V_g)/T$ of the $LaAlO_3/SrTiO_3$ interface at various gate voltages derived from Caviglia *et al.* [8]. The solid line marks the BKT behavior $R(V_g,T)/R_0(d) = \exp(-b_R(T/T_c - 1)^{-1/2})$ for a homogenous and infinite system with with $b_R = 3.43$. (b) Gate voltage dependence of the extrapolated transition line $T_c(V_g)$ and $R_0(V_g)$. The solid and dashed lines indicate the approach of T_c and R_0 to the extrapolated quantum phase transition.

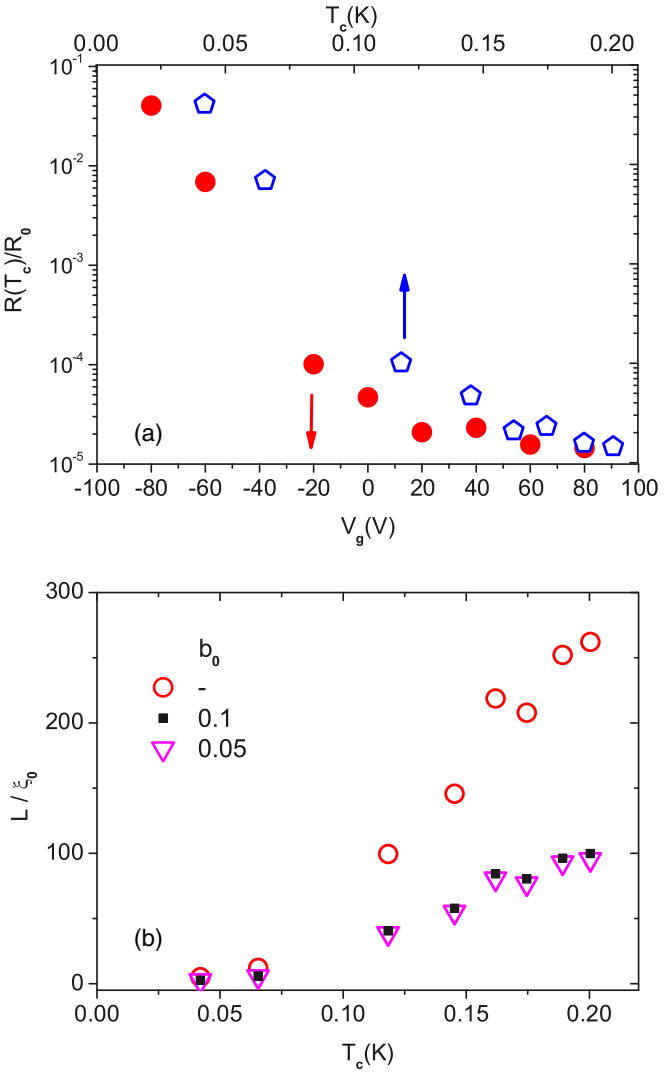

FIG. 9. (Color online) (a) $R(V_g,T)/R_0(V_g)$ vs T_c and gate voltage V_g of the LaAlO $_3$/$SrTiO_3$ interface derived from the data shown in Fig. (8); (b) Estimates for the ratio L/ξ_0 between correlation length and vortex core radius without the multiplicative logarithmic correction term (◯) and with this correction for different b_0 values entering Eq. (16).

$L_{\min}/\xi_0$. Figure 9(a) shows the T_c and d dependence of $R(V_g,T_c)/R_0(V_g)$ derived from Fig. 8(a). The resulting T_c dependence of L/ξ_{0-} is shown in Fig. 8(b) for $b_0 = 0.05$ and 0.1 in comparison with the absence of the multiplicative logarithmic correction. Note that $b_0 = 0.05$ is comparable to $b_0 \approx 0.07$, derived from large-scale numerical simulations [25]. In analogy to the Bi films, important features include the substantial decline L/ξ_0 with decreasing T_c, and the comparably low values of L/ξ, namely $L/\xi_0 < 100$ compared to the lower bound $L/\xi_0 \gtrsim 10^5$ emerging from the ^{4}He data shown in Fig. 2. According to this and in analogy to the Bi films the runaway from BKT behavior as observed in Fig. 9 is attributable to a limiting length L where the ratio L/ξ_0 decreases with reduced T_c. Nevertheless, there is a temperature range where consistency with BKT behavior is observed, but in a strict sense a normal state to superconductor BKT transition is suppressed.

An independent confirmation of the finite-size scenario demands the magnitude of L, allowing to determine ξ_0 and with that the temperature dependence of the correlation length $\xi_+(T)$, as well as $\xi_+(T^*) = L$, where the runaway from BKT behavior should occur. Given the previous estimate derived from the magnetic-field-induced finite-size effect [24]

$$L \simeq 490 \text{ Å}, \tag{23}$$

for a $LaAlO_3/SrTiO_3$ interface with $T_c \simeq 0.21$ we obtain with $L/\xi_0 \simeq 100$, taken from Fig. 9(b), for the vortex core radius the value

$$\xi_0 \simeq 4.9 \text{ Å}. \tag{24}$$

The resulting temperature dependence of the correlation length is shown in Fig. 10 in terms of $\xi_+(T)$ vs $t^{-1/2}$. As the correlation length cannot grow beyond L the runaway from BKT behavior should occur around the crossing point between $\xi_+(T)$ and L at $t^{-1/2} \simeq 2.69$ corresponding to $T_c/T \simeq 0.88$. A glance at Fig. 8(a) reveals that around this value the data

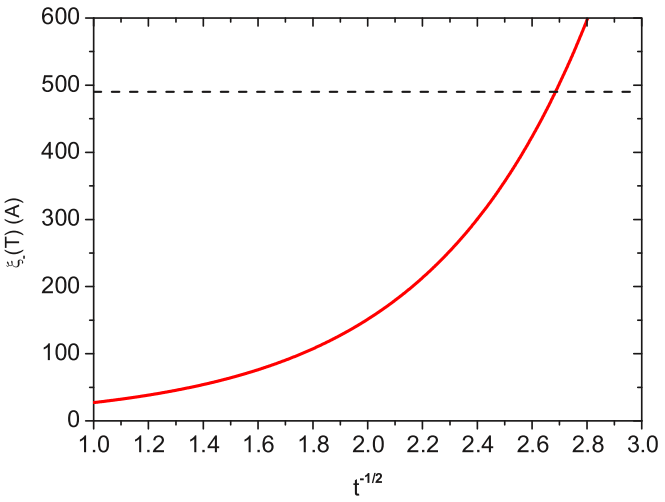

FIG. 10. (Color online) Correlation length $\xi_+(T) = \xi_0 \exp[2\pi/(bt^{1/2})]$ vs $t^{-1/2}$ of the $LaAlO_3/SrTiO_3$ interface with $T_c \simeq 0.21$ K for $\xi_0 = 4.9$ Å and $2\pi/b = b_R/2 = 1.72$. The dashed line marks $L = 208$ Å. The crossing point at $t^{-1/2} \simeq 2.69$ corresponds to $T_c/T \simeq 0.88$.

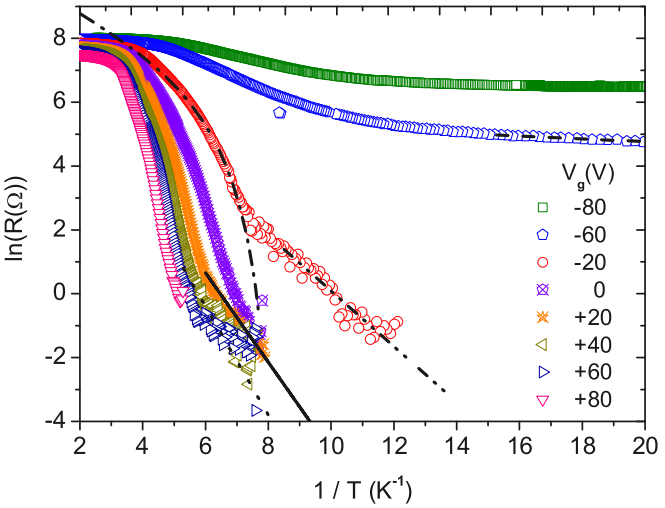

FIG. 11. (Color online) $\ln(R)$ vs $1/T$ of the $LaAlO_3/SrTiO_3$ interface for various gate voltages. The straight lines are Eq. (25): dashed line: $V_g = -60$ V with $r = 5.64$ and $s(T) = 0.044$ K; dash-dot-dot line: $V_g = -20$ V with $r = 8.78$ and $s(T) = 0.87$ K; full line: $V_g = +20$ V with $r = 9.06$ and $s(T) = 1.4$ K; dotted line: $V_g = +60$ V with $r = 9.8$ and $s(T) = 1.7$ K. The beginnings of the lines mark the respective $1/T_c$. The dash-dot line marks the BKT behavior (6) at $V_g = -20$ V with $R_0 = 44$ kΩ, $b_R = 3.43$ and $T_c = 0.119$ K.

of the $LaAlO_3$ /$SrTiO_3$ interface at gate voltage $V_g = 80$ V ($T_c \simeq 0.2$ K) run away from the BKT behavior. This agreement reveals that magnetic field and zero-field finite-size scaling yield consistent results. On this ground is the smeared BKT transition in both the Bi films and the $LaAlO_3/SrTiO_3$ interface attributable to a finite-size effect stemming from a limiting length L. In the samples with highest T_c its dimension is $L \simeq 208$ Å in the Bi films and $L \simeq 490$ Å in the $LaAlO_3/SrTiO_3$ interface.

Next we turn to the finite-size behavior below the extrapolated transition temperature. Here the limiting length L prevents the thermal length $\xi_-(|t|)$ from diverging. But compared to $\xi_+(|t|)$ the thermal length is much smaller for the same $|t|$ [Eq. (15)]. For this reason $L \gtrsim \xi_-(T)$ is expected to hold already slightly below T_c. In this regime the sheet resistance is controlled by the free vortex density where Eq. (13) rewritten in the form

$$\ln[R(T)] = r - \frac{s(T)}{T}, \quad s(T) = \frac{\pi J(T)}{k_B} \ln \frac{L}{\xi_0} \tag{25}$$

applies. Accordingly, the coefficient $s(T)$ controls deviations from the $1/T$ temperature dependence. At zero temperature the superfluid stiffness given by Eq. (9) is fixed by the magnetic penetration depth in terms of $J(T=0) \propto d/\lambda^2(T=0)$, expected to vanish as $J(T=0) \propto d/\lambda^2(T=0) \propto T_c$ [29]. On the other hand, approaching T_c from below, the superfluid stiffness tends according to Eq. (12) to $J(T_c^-) = 2k_B T_c/\pi$. In addition in both the Bi films [Fig. 4(b)] and the $LaAlO_3/SrTiO_3$ interface [Fig. 9(b)] $\ln(L/\xi_0)$ decreases with reduced T_c. As a consequence the magnitude of $s(T)$ is expected to decrease with reduced T_c. In Fig. 11, showing $\ln(R)$ vs $1/T$ of the $LaAlO_3/SrTiO_3$ interface for various gate voltages, we observe that this supposition is well confirmed. On the other hand, in the temperature regime of interest the data exhibit jitter masking the characteristic temperature dependence of the superfluid stiffness in $s(T)$ [14]. Indeed, the straight lines, corresponding to the nearly temperature-independent $s(T) \approx 2T_c \ln(L/\xi_0)$, describe the data quite well. To evidence the smeared BKT transition we included in Fig. 11 the characteristic BKT temperature dependence (6) in terms of the dash-dot-dot line. Additional confirmation of this finite-size scenario below T_c stems from the observation of an ohmic regime at small currents [7] because it uncovers according to Eq. (1) the presence of free vortices. The important implication then is: although BKT behavior is observable in an intermediate temperature regime above the extrapolated T_c, in a strict sense a BKT transition does not occur. It is smeared out and the sheet resistance vanishes at zero temperature only because Eq. (25) reduces in the zero-temperature limit to

$$R(T) = r \exp -\left(\frac{\pi J(T=0)}{k_B T} \ln \frac{L_{\rm lim}}{\xi_0}\right) = r\left(\frac{\xi_0}{L_{\rm min}}\right)^{\frac{\pi J(T=0)}{k_B T}}. \tag{26}$$

Contrariwise, the sheet resistance of the Bi films shown in Fig. 3 does not exhibit a significant temperature dependence below $T \approx T_c/2$ down to $T \approx T_c/10$. To disentangle the scaling regimes below T_c more quantitatively, we note that the plot $R(T)/R_0$ vs T_c/T should exhibit a crossover from a temperature-dependent to a temperature-independent regime at T^* where the diverging length $\xi_-(T)$ equals the limiting length $L_{\rm min}$. According to Eqs. (13) and (14) T^* follows from

$$\frac{L}{\xi_0} = \frac{\xi_-(T^*)}{\xi_0} = \exp\left(\frac{1}{b(1-T^*/T_c)^{1/2}}\right). \tag{27}$$

To estimate T^* we show in Fig. 12 the temperature dependence of $\xi_-(T)$ in terms of $\xi_-(T)/\xi_0$ vs T/T_c for the Bi films and

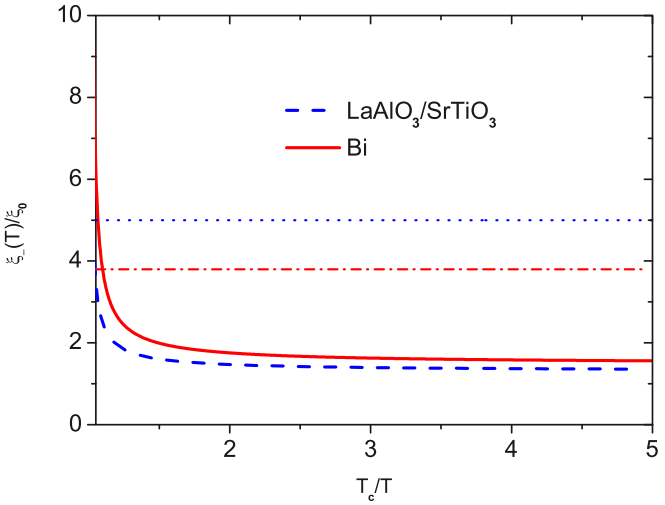

FIG. 12. (Color online) $\xi_-(T)/\xi_0 = \exp[1/(b(1-T/T_c)^{1/2})]$ vs T/T_c for the Bi films with $1/b = b_R/4\pi \simeq 0.398$ and the $LaAlO_3/SrTiO_3$ interface with $1/b = b_R/4\pi \simeq 0.273$. The dash dot and dotted lines mark the minimum value of L/ξ_0. $L/\xi_0 \simeq 3.8$ for the Bi films [Fig. 4(b)] and $L/\xi_0 \simeq 5$ for the $LaAlO_3/SrTiO_3$ interface [Fig. 9(b)].

the $LaAlO_3/SrTiO_3$ interface. Noting that the minimum value of L/ξ_0 in the Bi films is around 3.8 [Fig. 4(b)] and in the $LaAlO_3/SrTiO_3$ interface around around 5 [Fig. 9(b)] it becomes clear that in both systems T^* is close to and slightly below T_c. As a result, the temperature regime where $\xi_-(T) > L_{\rm lim}$ holds is restricted to temperatures very close to T_c only, while the regime where $\xi_-(T) < L$ applies sets in slightly below T_c. It is the regime where the sheet resistance adopts the characteristic temperature dependence given by Eq. (25). A glance at Fig. 11, showing $\ln(R)$ vs $1/T$ of the $LaAlO_3/SrTiO_3$ interface, uncovers agreement with this temperature dependence, while the sheet resistance of the Bi films shown in Fig. 3 does not exhibit a significant temperature dependence below $T \approx T_c/2$. Taking the saturation of the sheet resistance in the Bi films for granted it implies the breakdown of the BKT behavior below T_c, while it applies above T_c. The breakdown may then be a clue that below T_c a process is present, which destroys BKT behavior. On the other hand we have seen that the $LaAlO_3/SrTiO_3$ interface data is at and below T_c remarkably consistent with the predicted finite-size BKT behavior. However, the absence of BKT behavior below T_c is inconsistent with measurements of the superfluid stiffness [15–17], uncovering a smeared Nelson-Kosterlitz [14] jump near T_c and the presence of superfluidity down to the lowest attained temperatures. Given the odd behavior of the Bi films it should be kept in mind that a failure to cool the electrons in the low-temperature limit also implies a flattening of the sheet resistance [19]. On the other hand it has been argued that in the present case the measuring currents are far too low for heating to be the cause of flattening [6].

Finally, to explore the implications of a magnetic-field-induced finite-size effect below T_c we depicted in Fig. 13(a) the temperature dependence of the sheet resistance of a $LaAlO_3/SrTiO_3$ interface with $T_c \simeq 0.19$ K at various magnetic fields. Although the data exhibit jitter in the low field

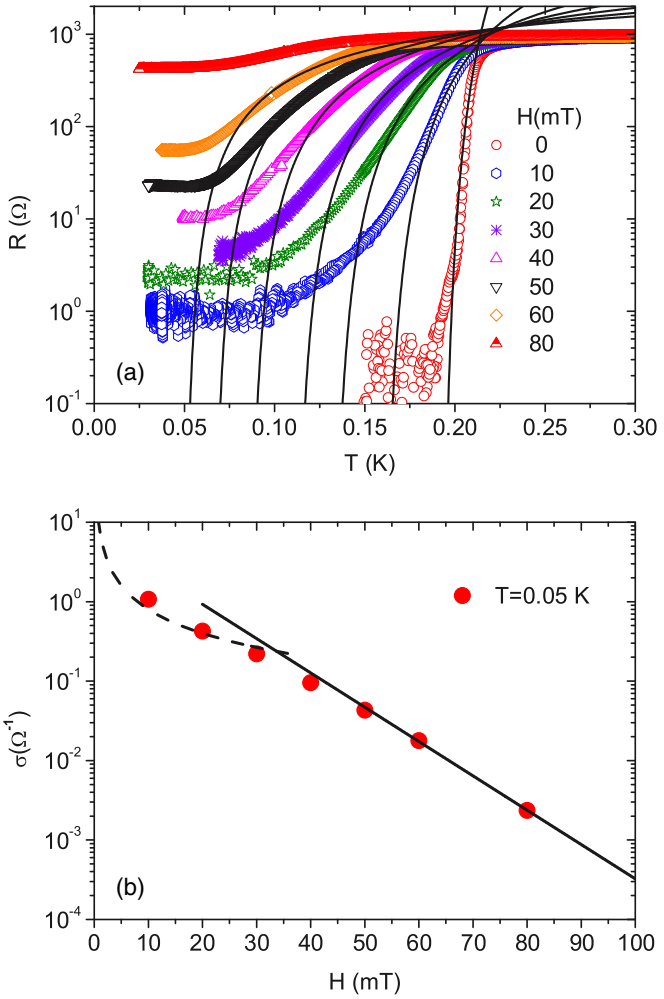

FIG. 13. (Color online) (a) Temperature dependence of the sheet resistance of a $LaAlO_3$ /$SrTiO_3$ interface with $T_c \simeq 0.19$ K at various magnetic fields applied perpendicular to the interface taken from Reyren *et al.* [49] The solid lines are fits to the BKT form (6) of the sheet resistance with $b_R = 3.43$ yielding for T_c and R_0 the estimates shown in Fig. 14; (b) Sheet conductivity vs H at $T = 0.05$ K. The solid line is the empirical form (22) with $\overline{\sigma}_0 = 6.79\ \Omega^{-1}$ and $\overline{a} = 0.099\ \mathrm{mT}^{-1}$. The dashed line is Eq. (18) in the from $\sigma = \widetilde{\sigma}/H$ where $\widetilde{\sigma} = 8\ (\Omega^{-1}\ \mathrm{mT})$.

limit the predicted saturation of the sheet resistance in the $T \to 0$ limit [Eq. (18)] is well established. On the other hand, considering the isotherm shown in Fig. 13(b), the consistency with the finite-size behavior (18) is restricted to low temperatures and low fields. Above $H = 30$ mT a crossover to the empirical form (22) can be surmised as the crossing point of the isotherms around $H_c = 110$ mT is approached. This crossing point is the direct consequence of the fact that in the covered T range R decreases with decreasing T for $H < H_c$, increases with decreasing T for $H > H_c$, and is T independent at H_c. Noting that the scaling form (18) presumes that density fluctuations are small [25], which is true for large limiting lengths $L_H = (\Phi_0/aH)^{1/2}$, but not for small, it becomes clear that the applicability of this approach is limited to the low field limit. Another essential feature emerging from Fig. 13(a) is the shift of the sheet resistance

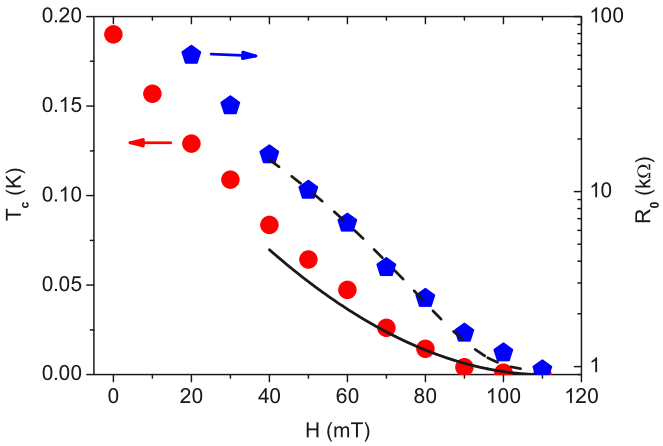

FIG. 14. (Color online) Estimates for T_c and R_0 resulting from the fits to the BKT form (6) of the sheet resistance included in Fig. 13(a). The solid line is $T_c = T_0(H_c - H)^{z\overline{\nu}}$ with $T_0 = 3 \times 10^{-5}$ $(\mathrm{KmT})^{1/z\overline{\nu}}$, $H_c = 110$ mT, $z\overline{\nu} = 1.92 \pm 0.1$ and the dashed line is $R_0 = R_{0c} + \overline{R}(H_c - H)^{2\overline{\nu}}$ with $R_{0c} = 0.96$ kΩ, $\overline{R} = 0.106\ \Omega\ \mathrm{mT}^{1/2\overline{\nu}}$, and $2\overline{\nu} = 2.78$. These lines indicate the approach to the extrapolated quantum critical point.

curves to lower temperatures with increasing magnetic field. This behavior uncovers the pair-breaking effect of the magnetic field leading in a mean-field treatment to a reduction of T_{c0} according to $T_{c0}(H = 0) - T_{c0}(H) \propto H$ [50–52]. Adopting the finite-size point of view this behavior relies on the fact that an applied magnetic field sets an additional limiting length $L_H = (\Phi_0/aH)^{1/2}$, giving rise to a smeared BKT transition at a fictitious BKT transition temperature $T_c(H)$ below $T_c(H = 0)$. Contrariwise, in the standard finite-size effect one attains T_c in the $L \to \infty$ limit only. To quantify this option we performed fits to the characteristic BKT form (6) of the sheet resistance. A glance at Fig. 13(a) reveals, in analogy to the zero-field case [Fig. 8(a)], agreement in an intermediate temperature range below $T_c(H)$.

Given the consistency with the BKT expression (6) and Fig. 13(a) estimates for the fictitious lines $T_c(H)$ and $R_0(H)$ are readily obtained and shown in Fig. 14. $T_c(H)$ extrapolates to zero around $H_c = 110$ mT where the isotherms cross. This behavior suggests a magnetic-field-induced quantum phase transition where superconducting behavior is lost at zero temperature and the amplitude R_0 approaches the critical value $R_0(H_c) \simeq 1$ kΩ which is close to the normal state sheet resistance at $T = 0.5$ K. We note that $T_c(H)$ has properties compatible with a quantum critical point, where $T_c = T_0(H_c - H)^{z\overline{\nu}}$ applies [36]. z is the dynamic and $\overline{\nu}$ the critical exponent of the zero-temperature correlation length. The power law fit included in Fig. 14 yields $z\overline{\nu} = 1.92 \pm 0.1$. It is interesting to note that this value is comparable with transport studies including MoGe [11], $Nb_{0.15}Si_{0.85}$ [53], InO_x [54], and $LaAlO_3/SrTiO_3$ interface [55] samples, though these studies have limited their analysis to exclude resistance data showing flattening in the zero temperature limit. In any case, BKT behavior occurs in an intermediate temperature range only. The extrapolated BKT line $T_c(H)$ is not attainable because the magnetic-field-induced finite-size effect [Eq. (18)] generates, as observed in Fig. 13(a), the flattening out of the sheet resistance in the $T \to 0$ limit. Nevertheless, the established survival of BKT behavior in a magnetic field applied perpendicular to the film also implies a smeared sudden drop in the superfluid stiffness at $T_c(H)$, where the superfluid stiffness adopts the universal value given by the Nelson-Kosterlitz relation (12). Recently, this behavior has been observed in MoGe and InO_x thin films by means of low-frequency measurements of the ac conductivity [17]. Although the low frequency $f = 20$ kHz implies an additional limiting length, namely $L_f \propto f^{-1/2}$, the magnetic field dependence of the blurred Nelson-Kosterlitz jump has been clearly detected and the power law fits to $T_c(H)$ yielded for $z\overline{\nu}$ the estimates 1.25 ± 0.25 for MoGe and 1.3 ± 0.4 for InO_x.

Lastly we consider the limitations of the quantum scaling form [36]

$$R(H,T) = R_c G(x), \quad x = \frac{H_c - H}{T^{1/z\overline{\nu}}}, \tag{28}$$

applicable close to the quantum critical point. $G(x)$ is a scaling function of its argument and $G(0) = 1$. It is essentially a finite-size scaling function. Indeed at finite temperatures it is the divergence of the zero-temperature correlation length $\xi(T = 0) \propto (H_c - H)^{-\overline{\nu}}$ cut off by the thermal length $L_T \propto T^{-1/z}$ so that $x \propto [L_T/\xi(T = 0)]^{1/\overline{\nu}} \propto (H_c - H)/T^{1/z\overline{\nu}}T$. The data for $R(H,T)$ plotted vs $x = (H_c - H)/T^{1/z\overline{\nu}}$ should then collapse on a single curve. On the other hand BKT behavior uncovered in Fig. 13(a) implies the scaling form (6) rewritten in the form

$$R(H,T) = R_0(H)\exp(-b_R/(T/T_c(H) - 1)^{1/2}), \tag{29}$$

where $T_c(H) = T_0(H_c - H)^{z\overline{\nu}}$ is the transition line shown in Fig. 14. Noting that

$$\frac{T}{T_c(H)} = \frac{1}{T_0 x^{z\overline{\nu}}}, \tag{30}$$

BKT behavior leads with Eqs. (28) and (29) to the explicit scaling form

$$R(H,T) = R_0(H)\exp(-b_R/((T_0 x^{z\overline{\nu}})^{-1} - 1)^{1/2}), \tag{31}$$

valid for any $T/T_c(H) = (T_0 x^{z\overline{\nu}})^{-1} > 1$ where the universal critical behavior is entirely classical. The scaling plot $R(H,T)$ vs $z = (H_c - H)/T^{1/z\overline{\nu}}$ obtained from the $LaAlO_3/SrTiO_3$ interface sheet resistance data shown in Fig. 13(a) is depicted in Fig. 15(a). For comparison we included the BKT scaling form (31). Apparently, the data do not collapse on a single curve because the amplitude R_0 exhibits a pronounced field dependence (see Fig. 14) and the sheet resistance flattens out for large and small values of the scaling argument z. For fixed $H_c - H$ this reflects the observed flattening out of the sheet resistance in the low- and high-temperature limits [Fig. 13(a)]. A glance at Fig. 15(b) reveals that an improved data collapse is achieved by taking the field dependence of the amplitude R_0 into account. Clearly, the flattening out for small and large z values remains. Noting that for fixed $H_c - H$ small z values are attainable at rather high temperatures only, the respective saturation reflects the fact that in this temperature regime BKT fluctuations no longer dominate. On the other hand large scaling arguments require the incidence of the zero-temperature limit where the magnetic-field-induced finite-size effect leads to a flattening out in the temperature dependence and with that in the z dependence of the sheet resistance in

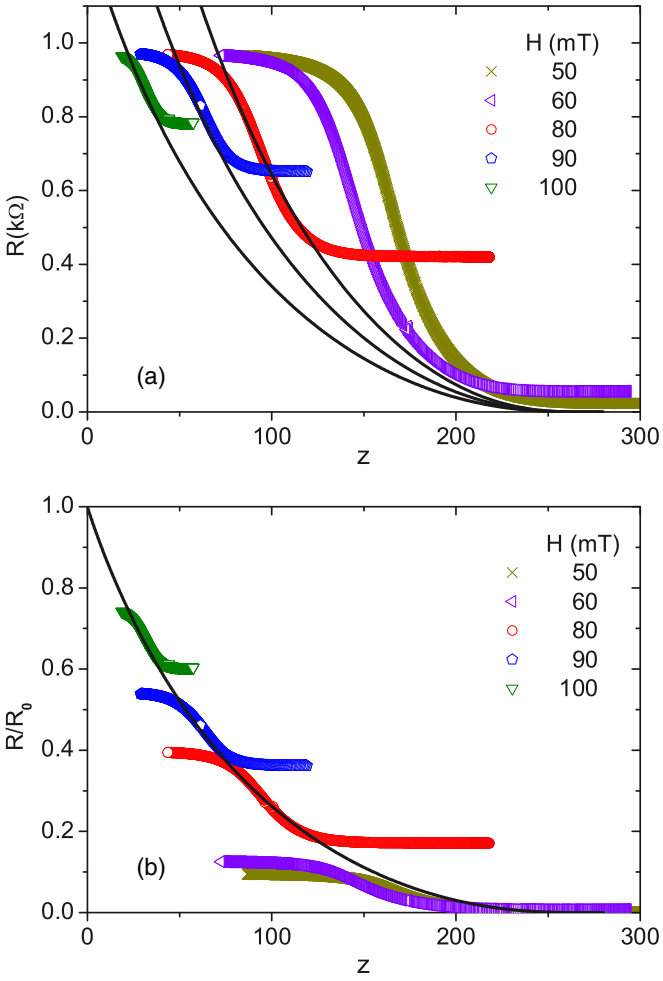

FIG. 15. (Color online) (a) Scaling plot $R(H,T)$ vs $z = (H_c - H)/T^{1/z\bar{\nu}}$ with $H_c = 110$ mT, $z\bar{\nu} = 1.92$, and $b_R = 3.43$. The solid lines mark the respective BKT scaling form (31) with $R_0(H)$ taken from Fig. 14 and $T_0 = 2 \times 10^{-5}$ (KmT)$^{1/z\bar{\nu}}$. (b) Scaling plot $R(H,T)/R_0(H)$ vs $z = (H_c - H)/T^{1/z\bar{\nu}}$. The solid line is the BKT scaling form (31).

the $z \to \infty$ limit. Furthermore, the field dependence of the amplitude R_0 (Fig. 14) also implies that the quantum scaling form holds in a unattainable regime close to quantum criticality only ($R_0 \to R_{0c}$).

III. SUMMARY AND DISCUSSION

We analyzed sheet resistance data of thin Bi films [6] and the $LaAlO_3/SrTiO_3$ interface [8,49] near the onset of superconductivity to explore the compatibility with BKT behavior. On the Bi films the onset temperature has been tuned by the film thickness, while on the $LaAlO_3/SrTiO_3$ interface the gate voltage and the magnetic field, applied perpendicular to the interface, acted as tuning parameter. Noting that BKT behavior involves the transition from a low-temperature state in which only paired vortices exist to a high-temperature state in which free vortices occur, we demonstrated that finite-size-induced free vortices below T_c prevent the occurrence of a BKT transition in a strict sense. This does not mean, however, that the BKT vortex-unbinding mechanism does not occur and is not observable. Indeed our finite-size analysis revealed that BKT behavior is present in an intermediate temperature range above the extrapolated BKT transition temperature. This temperature range depends on the magnitude of the limiting length L while the extrapolated transition temperature corresponds to the limit $L \to \infty$. Limiting lengths include the effective magnetic penetration depth $\lambda_{2D} = \lambda^2/d$, the dimension L_h of the homogeneous domains in the sample, the magnetic length $L_H \propto (\Phi_0/H)^{1/2}$, and in the case of ac measurements $L_f \propto f^{-1/2}$. $L = \min[\lambda_{2D}, L_h, L_H, L_f]$ controls the density of free vortices n_F, which determines the sheet resistance ($R \propto n_F$) as well as the correlation length ($\xi \propto n_F^{-1/2}$) at and above T_c. In this temperature range the limiting lengths prevent the correlation length to diverge. Concentrating on the dc sheet resistance we analyzed the data using finite-size scaling formulas appropriate for the BKT transition [24,25].

The main results for zero magnetic fields include: Above T_c we observed in an intermediate temperature range consistency with the characteristic BKT behavior and a thickness-dependent or gate-voltage-dependent BKT transition temperature T_c [Figs. 1(a) and 8(a)]. However, in analogy to finite systems, the measured sheet resistance does not vanish at T_c. In this context it should be kept in mind that there is the Harris criterion [26,27], stating that short-range correlated and uncorrelated disorder is irrelevant at the unperturbed critical point, provided that $\nu > 2/D$, where D is the dimensionality of the system and ν the critical exponent of the finite-temperature correlation length. With $D = 2$ and $\nu = \infty$, appropriate for the BKT transition [22], this disorder should be irrelevant. Accordingly, the nonvanishing sheet resistance at T_c points to a finite-size-induced smeared BKT transition. Invoking the finite-size scaling formula for the sheet resistance at T_c we obtained estimates for the T_c dependence of the ratio between the limiting length and the vortex core radius, namely L/ξ_0 [Figs. 3(b) and 9(b)]. Striking features included the substantial decline of $L/\xi_0|_{\max} \approx 10^2$ with decreasing T_c and in comparison with $L/\xi_0 \gtrsim 10^5$ in ^{4}He the low value of $L/\xi_0|_{\max}$. This difference and the T_c dependence of L/ξ_0 imply enhanced smearing of the BKT transition with reduced T_c as observed [Figs. 1(a), 3, and 8(a)]. To disentangle the T_c dependence of the limiting length L and the vortex core radius ξ_0 we invoked the magnetic-field-induced finite-size effect allowing us to estimate the limiting length directly from magnetic field dependence of the sheet conductivity at fixed temperature below T_c [24]. Unfortunately, in both the Bi films and the $LaAlO_3/SrTiO_3$ interface, the necessary data is available for the samples with highest T_c only. For the 23.42 Å thick Bi film we obtained $L \simeq 208$ Å, $\xi_0 \simeq 6.5$ Å [Eqs. (20) and (21)] and for the $LaAlO_3/SrTiO_3$ interface with $T_c \simeq 0.21$ K the estimates $L \simeq 490$ Å, $\xi_0 \simeq 4.9$ Å [Eqs. (23) and (24)]. These values for the extent of the homogeneous domains are comparable with the dimension of the superconducting patches emerging from scanning tunneling spectroscopy investigations on TiNi [46] and InO_x [47] films, as well as with scanning SQUID measurements at the interface $LaAlO_3/SrTiO_3$ [48]. To disentangle the T_c dependence of L and ξ_0 we used the empirical relationship $\xi_0 \propto T_c^{-1/z}$ with $z = 2$ [44,45], revealing that the extent of the homogenous domains decreases substantially with reduced T_c (Fig. 7). Accordingly the

enhanced smearing of the BKT transition with reduced T_c was traced back to the reduction of the limiting length L and the increase of the vortex core radius ξ_0 with decreasing T_c.

In the low-temperature limit and zero magnetic field we observed on the LaAlO $_3$/$SrTiO_3$ interface consistency with the characteristic finite-size scaling form (25) while the Bi films do not exhibit a significant temperature dependence below $T \approx T_c/2$. Taking the saturation of the sheet resistance in the Bi films for granted it implies the breakdown of BKT finite-size scaling below T_c, while it applies above T_c. The breakdown may then be a clue that below T_c a process is present, which destroys BKT behavior. On the other hand we have seen that the $LaAlO_3$ /$SrTiO_3$ interface data is at and below T_c remarkably consistent with the predicted finite-size BKT predictions. In addition, an absence of BKT behavior below T_c is also incompatible with measurements of the superfluid stiffness [15–17], uncovering a smeared Nelson-Kosterlitz [14] jump near T_c and the presence of superfluidity down to the lowest attained temperatures.

Subsequently we explored the implications of the magnetic-field-induced finite-size effect. Considering the temperature dependence of the sheet resistance at various magnetic fields, applied perpendicular to the interface of $LaAlO_3/SrTiO_3$, we observed in an intermediate temperature range remarkable consistency with the characteristic BKT form (6) [Fig. 13(a)]. Fits yielded the fictitious transition line $T_c(H)$ extrapolating to zero at $H_c \simeq 110$ mT where a quantum phase transition is expected to occur (Fig. 14). Indeed, $T_c(H)$ revealed properties compatible with a quantum critical point, near which $T_c = T_0(H_c - H)^{z\overline{\nu}}$ applies [36]. z is the dynamic and $\overline{\nu}$ the critical exponent of the zero-temperature correlation length. A power law fit yielded $z\overline{\nu} = 1.92 \pm 0.1$. However, this extrapolated line is not attainable because the magnetic-field-induced finite-size effect [Eq. (18)] generates the observed flattening out of the sheet resistance in the $T \to 0$ limit [Fig. 13(b)]. This feature has been observed in the 23.42 Å thick Bi film as well [6]. The survival of BKT behavior in applied magnetic fields also implies a smeared sudden drop in the superfluid stiffness at $T_c(H)$, where it adopts the universal value given by the Nelson-Kosterlitz relation (12). Recently, this behavior has been observed in MoGe and InO_x thin films by means of low-frequency measurements of the ac conductivity [17].

A key question our analysis raises is whether the homogeneity of two-dimensional superconductors can be improved to reach the quality of ^{4}He films. Analyzing the sheet resistance data of Bi films and the $LaAlO_3/SrTiO_3$ we have shown that the data are consistent with a finite-size effect attributable to the limited homogeneity of the samples. The limited length of the homogenous domains impedes the occurrence of a BKT and quantum phase transitions in the strict sense of a true continuous phase transition. However, this strict interpretation of the definition of a continuous phase transition does not imply that the BKT vortex-unbinding mechanism is not observable and the reduction of the extrapolated T_c does not reveal properties compatible with a quantum critical point. Indeed, notwithstanding the comparatively small dimension of the homogeneous domains, our finite-size analysis revealed reasonable compatibility with BKT and quantum critical point behavior. However, the reduction of the limiting length with decreasing T_c is an essential drawback (Fig. 7). Furthermore, considering the expected magnetic field tuned quantum phase transition in the $LaAlO_3/SrTiO_3$ interface, it was shown that the standard quantum scaling form (28) of the sheet resistance applies very close to the unattainable quantum critical point only (Fig. 15). Indeed, combining the BKT expression for the sheet resistance with the quantum scaling form of the extrapolated transition line $T_c(H)$, we derived the explicit scaling relation (31) uncovering the limitations of the standard quantum scaling form. Its main drawback was traced back to the neglect of the magnetic field dependence of the critical amplitude R_0, which varies substantially by approaching the critical value R_{0c} (Fig. 14).

Finally it should be noted that the finite-size scaling approach adopted here is compatible with the Harris criterion [26,27], stating that short-range correlated and uncorrelated disorder is irrelevant at the BKT critical point, contrary to approaches where the smearing of the BKT transition is attributed to a Gaussian-like distribution of the bare superfluid-stiffness around a given mean value [28]. The irrelevance of this disorder implies that the universal BKT properties still apply, while the nonuniversal parameters, including T_c, the vortex core radius ξ_0, and the amplitude R_0, may change. Contrariwise, the relevance of disorder at the extrapolated quantum phase transition, separating the superconducting and metallic phase, depends on the universality to which it belongs. The relevance of disorder is again controlled by the Harris criterion [26,27]: if the zero-temperature correlation length critical exponent fulfils the Harris inequality $\overline{\nu} > 2/D = 1$ the disorder does not affect the quantum critical behavior. Conversely, if $\overline{\nu} < 2/D = 1$ disorder is relevant and affects the nonuniversal parameters R_0 and T_c in the BKT form (2) of the sheet resistance and in particular the reduction of T_c. In the magnetic field tuned case, the field dependence of R_0 and T_c is attributable to Cooper-pair breaking. However, another important feature of the of $LaAlO_3/SrTiO_3$ interface is the large Rashba spin orbit interaction, which originates from the broken inversion symmetry. It has been shown that its magnitude increases with reduced T_c [56], suggesting that pair breaking occurs in zero magnetic field as well. Indeed, torque magnetometry measurement revealed that the $LaAlO_3/SrTiO_3$ interface has a magnetic moment, which points in the plane, and has an onset temperature that is at least as high as 40 K and persists below the BKT transition temperature [57].

ACKNOWLEDGMENTS

The authors acknowledge stimulating and helpful discussions with K. A. Müller and very useful comments from Stefano Gargilio.

[1] N. Markovic, C. Christiansen, A. Mack, and A. M. Goldman, Phys. Status Solidi B **218**, 221 (2000).
[2] A. M. Goldman, Physica E **18**, 1 (2003).
[3] V. F. Gantmakher and V. T. Dolgopolov, Phys. Usp. **53**, 1 (2010).
[4] A. M. Goldman, Int. J. Mod. Phys. B **24**, 4081 (2010).

[5] H. M. Jaeger, D. B. Haviland, B. G. Orr, and A. M. Goldman, Phys. Rev. B **40**, 182 (1989).

[6] Yen-Hsiang Lin, J. J. Nelson, and A. M. Goldman, Phys. Rev. Lett. **109**, 017002 (2012).

[7] N. Reyren, S. Thiel, A. D. Caviglia, L. Fitting Kourkoutis, G. Hammerl, C. Richter, C. W. Schneider, T. Kopp, A.-S. Rüetschi, D. Jaccard, M. Gabay, D. A. Muller, J.-M. Triscone, and J. Mannhart, Science **317**, 1196 (2007).

[8] A. D. Caviglia, S. Gariglio, N. Reyren, D. Jaccard, T. Schneider, M. Gabay, S. Thiel, G. Hammerl, J. Mannhart, and J.-M. Triscone, Nature (London) **456**, 624 (2008).

[9] T. Schneider, A. D. Caviglia, S. Gariglio, N. Reyren, and J.-M. Triscone, Phys. Rev. B **79**, 184502 (2009).

[10] D. Ephron, A. Yazdani, A. Kapitulnik, and M. R. Beasley, Phys. Rev. Lett. **76**, 1529 (1996).

[11] N. Mason and A. Kapitulnik, Phys. Rev. Lett. **82**, 5341 (1999).

[12] Y. Qin, C. L. Vicente, and J. Yoon, Phys. Rev. B **73**, 100505 (2006).

[13] Wei Liu, Li Dong Pan, Jiajia Wen, Minsoo Kim, G. Sambandamurthy, and N. P. Armitage, Phys. Rev. Lett. **111**, 067003 (2013).

[14] D. R. Nelson and J. M. Kosterlitz, Phys. Rev. Lett. **39**, 1201 (1977).

[15] S. J. Turneaure, Th. R. Lemberger, and J. M. Graybeal, Phys. Rev. B **63**, 174505 (2001).

[16] J. A. Bert, K. C. Nowack, B. Kalisky, H. Noad, J. R. Kirtley, Ch. Bell, Hiroki K. Sato, M. Hosoda, Y. Hikita, H. Y. Hwang, and K. A. Moler, Phys. Rev. B **86**, 060503(R) (2012).

[17] S. Misra, L. Urban, M. Kim, G. Sambandamurthy, and A. Yazdani, Phys. Rev. Lett. **110**, 037002 (2013).

[18] D. Dalidovich and P. Phillips, Phys. Rev. Lett. **89**, 027001 (2002).

[19] K. A. Parendo, K. H. Sarwa, B. Tan, and A. M. Goldman, Phys. Rev. B **74**, 134517 (2006).

[20] M. R. Beasley, J. E. Mooij, and T. P. Orlando, Phys. Rev. Lett. **42**, 1165 (1979).

[21] V. L. Berezinskii, Sov. Phys. JETP **32**, 493 (1971).

[22] J. M. Kosterlitz and D. J. Thouless, J. Phys. C **6**, 1181 (1973).

[23] J. Pearl, Appl. Phys. Lett. **5**, 65 (1964).

[24] T. Schneider, Phys. Rev. B **80**, 214507 (2009).

[25] A. Andersson and J. Lidmar, Phys. Rev. B **87**, 224506 (2013).

[26] A. B. Harris, J. Phys. C **7**, 1671 (1974).

[27] A. Aharony and A. B. Harris, Phys. Rev. Lett. **77**, 3700 (1996).

[28] L. Benfatto, C. Castellani, and T. Giamarchi, Phys. Rev. B **80**, 214506 (2009).

[29] T. Schneider and S. Weyeneth, J. Phys.: Condens. Matter **25**, 305701 (2013).

[30] T. Schneider and S. Weyeneth, J. Supercond. Nov. Magn. **26**, 3423 (2013).

[31] A. F. Hebard and A. T. Fiory, Phys. Rev. Lett. **50**, 1603 (1983).

[32] J. M. Repaci, C. Kwon, Qi Li, Xiuguang Jiang, T. Venkatessan, R. E. Glover, C. J. Lobb, and R. S. Newrock, Phys. Rev. B **54**, R9674 (1996).

[33] S. T. Herbert, Y. Jun, R. S. Newrock, C. J. Lobb, K. Ravindran, H.-K. Shin, D. B. Mast, and S. Elhamri, Phys. Rev. B **57**, 1154 (1998).

[34] R. W. Crane, N. P. Armitage, A. Johansson, G. Sambandamurthy, D. Shahar, and G. Grüner, Phys. Rev. B **75**, 094506 (2007).

[35] Weiwei Zhao *et al.*, Solid State Commun. **165**, 59 (2013).

[36] S. L. Sondhi, S. M. Girvin, J. P. Carini, and D. Shahar, Rev. Mod. Phys. **69**, 315 (1997).

[37] B. I. Halperin and D. R. Nelson, J. Low Temp. Phys. **36**, 599 (1979).

[38] D. S. Fisher, M. P. A. Fisher, and D. A. Huse, Phys. Rev. B **43**, 130 (1991).

[39] V. Ambegaokar, B. I. Halperin, D. R. Nelson, and E. D. Siggia, Phys. Rev. B **21**, 1806 (1980).

[40] L. M. Steele, C. J. Yeager, and D. Finotello, Phys. Rev. Lett. **71**, 3673 (1993).

[41] G. Agnolet, S. L. Teitel, and J. D. Reppy, Phys. Rev. Lett. **47**, 1537 (1981).

[42] H. J. Jensen (unpublished).

[43] K. Medvedyeva, B. J. Kim, and P. Minnhagen, Phys. Rev. B **62**, 14531 (2000).

[44] D. Finotello and F. M. Gasparini, Phys. Rev. Lett. **55**, 2156 (1985).

[45] H. Cho and G. A. Williams, Phys. Rev. Lett. **75**, 1562 (1995).

[46] B. Sacépé, C. Chapelier, T. I. Baturina, V. M. Vinokur, M. R. Baklanov, and M. Sanquer, Phys. Rev. Lett. **101**, 157006 (2008).

[47] B. Sacépé, T. Dubouchet, C. Chapelier, M. Sanquer, M. Ovadia, D. Shahar, M. Feigel'man, and L. Ioffe, Nature Phys. **7**, 239 (2011).

[48] J. A. Bert, B. Kalisky, Ch. Bell, M. Kim, Y. Hikita, H. Y. Hwang, and K. A. Moler, Nature Phys. **7**, 767 (2011).

[49] N. Reyren, S. Gariglio, A. D. Caviglia, D. Jaccard, T. Schneider, and J.-M. Triscone, Appl. Phys. Lett. **94**, 112506 (2009).

[50] A. A. Abrikosov and L. P. Gor'kov, Sov. Phys. JETP **12**, 1243 (1961).

[51] K. Aoi, R. Meservey, and P. M. Tedrow, Phys. Rev. B **9**, 875 (1974).

[52] N. Shah and A. Lopatin, Phys. Rev. B **76**, 094511 (2007).

[53] H. Aubin, C. A. Marrache-Kikuchi, A. Pourret, K. Behnia, L. Bergé, L. Dumoulin, and J. Lesueur, Phys. Rev. B **73**, 094521 (2006).

[54] A. F. Hebard and M. A. Paalanen, Phys. Rev. Lett. **65**, 927 (1990).

[55] J. Biscaras, N. Bergeal, S. Hurand, C. Feuillet-Palma, A. Rastogi, R. C. Budhani, M. Grilli, S. Caprara, and J. Lesueur, Nature Mater. **12**, 542 (2013).

[56] A. D. Caviglia, M. Gabay, S. Gariglio, N. Reyren, C. Cancellieri, and J.-M. Triscone, Phys. Rev. Lett. **104**, 126803 (2010).

[57] L. Li, C. Richter, J. Mannhart, and R. C. Ashoori, Nature Phys. **7**, 762 (2011).